Computer Simulation Studies of Molecular Orientation and the Stress−Optical Properties of Polyethylene Networks

D. J. R. Taylor* and R. F. T. Stepto

Polymer Science & Technology Group, Manchester Materials Science Centre, UMIST & University of Manchester, Grosvenor Street, Manchester M1 7HS, U.K.

R. A. Jones and I. M. Ward

IRC in Polymer Science & Technology, Department of Physics, University of Leeds, Leeds LS2 9JT, U.K.

Received March 30, 1998; Revised Manuscript Received December 21, 1998

ABSTRACT: A new Monte Carlo (MC) method is used to interpret experimental stress−optical coefficients (C) of polyethylene (PE) networks in uniaxial deformation. The method considers the deformation of individual PE-network chains, whose conformational properties and $-CH_2-$ segment orientations are calculated using a rotational-isomeric-state (RIS) model. Individual chains, randomly oriented in three dimensions, are deformed uniaxially and affinely, but only up to the maximum chain-extension, consistent with $W(r) = 0$, where $W(r)$ is the radial end-to-end distance distribution. The changes in network elastic free-energy, and in the average orientation of $-CH_2-$ segment vectors with respect to the deformation axis are evaluated. The MC method gives, in agreement with experiment, values of C that are dependent upon both deformation ratio, λ, and on network-chain length. Furthermore, the method shows that a single equivalent freely jointed chain cannot be used to describe *both* stress−optical and stress−strain behaviors.

Introduction

The photoelastic properties of elastomeric networks received particular attention in the period 1945−1970, due to the studies of Treloar, Saunders, Gent, and their collaborators on rubbers and cross-linked polyethylenes. The starting point for an understanding of the development of optical anisotropy with strain was the 1942 theory of Kuhn and Grün.[1] This theory replaces the true molecular network by an idealized network of ν identical chains, each of which consists of m freely jointed links of length l'. They are equivalent random links in that any valence-angle and rotational-barrier restrictions are accounted for by the matching of this hypothetical chain to the real chain. Junction points are assumed to deform affinely, and any effects due to intermolecular interactions are assumed to be negligible. The simplest interpretation of the development of optical anisotropy with strain was based on a network of Gaussian, freely jointed chains, and for strains which are not too large, both birefringence, $\Delta\tilde{n}$, and true stress, t, are proportional to $\lambda^2 - \lambda^{-1}$, where λ is the uniaxial deformation ratio. Hence, for a constant number of real bonds per equivalent random link, there is a constant stress−optical coefficient, defined as $\Delta\tilde{n}/t$.

It was soon recognized that the Gaussian network model was inadequate because a constant stress−optical coefficient did not apply. Early attempts to deal with this issue on the basis of the inverse Langevin function have been well described by Treloar[2] and by Saunders and co-workers.[3] These studies left some major issues unresolved, partly due to uncertainties in predicting accurate values for bond polarizabilities, which are essential in relating the calculated segmental orientations to experimental birefringence measurements, and partly due to uncertainties in dealing with the issue of some chains in a network becoming fully extended.

In more recent studies, Ward and co-workers[4] used stress−optical measurements to gain an understanding of the molecular mechanism of the deformation of poly(ethylene terephthalate) (PET) and have used the Kuhn and Grün theory to analyze deformation in both the glassy and the rubbery states. Although strictly applicable to moderate deformations only, the equivalent random-link model for PET suggested that a substantial proportion of the network chains had become fully extended at comparatively low draw ratios. The development of a treatment of optical anisotropy for such a case was modeled by Nobbs and Bower,[5] who added to the basic Kuhn and Grün model in order that it could be applied to larger macroscopic deformations. They proposed that fully extended chains rotated according to the affine deformation scheme but ignored any changes in the lengths of the rotating vector lines. This has been called pseudoaffine deformation, and corresponds to that proposed by Kratky[6] for crystals in semicrystalline polymers. However, the approach is still limited by the fact that real chains are replaced by freely jointed ones.

At about the same time, the constrained-junction theory of Flory[7] was further developed by Flory and Erman[8] to treat the strain−birefringence behavior of poly(dimethyl siloxane) (PDMS) networks. The model is also based on a network of equivalent freely jointed chains, with no limit on maximum chain extension. The constraints imposed on the fluctuations of junctions in the real network are assumed to decrease with increasing macroscopic deformation, and many comparisons with experimental stress−strain and stress−optical data[8,9] have been made. However, some of the adjustable parameters used in the theory have no clear physical interpretations (although they are described as "molecular" quantities), and the analysis fails to elucidate clearly the molecular phenomena responsible for observed network stress−optical behavior. Furthermore, the network-chain-length dependence of $\Delta\tilde{n}/t$, which is observed experimentally, can only be reproduced by

10.1021/ma9805001 CCC: $18.00
Published on Web 03/04/1999

invoking a dependence of the parameter κ upon network-chain molar-mass.[10]

More recent investigations,[11−17] in which molecular orientation during network deformation is measured *directly* (using techniques such as NMR and infrared dichroism), show the effects of network-chain structure on segmental orientation. In one such study,[11] the $P_2(\zeta)$ function (see later) for a series of PDMS networks was measured using infrared dichroism. The experimental data were analyzed using a rotational-isomeric-state (RIS) model for an individual PDMS network chain,[12] thus avoiding the ambiguities associated with the definition of an equivalent freely jointed link. However, this approach did not include the effects of maximum chain extensibility. The detailed RIS approach showed that segmental orientation in PDMS networks is grossly overestimated by the Kuhn and Grün model, based upon equivalent chains defined using a moment-matching technique.[18] Furthermore, the good agreement between experimental values of $P_2(\zeta)$ and those calculated using the single-chain RIS model suggested that intermolecular interactions were negligible in the PDMS networks studied. However, PDMS-network deformation experiments carried out using NMR,[13,15] and subsequent theoretical analyses,[14−17] have shown that intermolecular interactions *increase* the segmental orientation. The resulting increase in $P_2(\zeta)$ relative to that expected in the absence of intermolecular interactions will be discussed in more detail later in this paper.

The recently developed Monte Carlo (MC) network model of Stepto and Taylor[19,20] is based on detailed molecular representations of network-chain structures, and also addresses the problem of chains in a rubbery network becoming fully extended. Chains are deformed individually and maximum chain extension is restricted, consistent with $W(r) = 0$, where $W(r)$ is the network-chain radial end-to-end distance distribution, generated using an RIS chain model. The approach has been shown to reproduce the experimentally observed, uniaxial stress−strain behavior of PDMS.[19] An increase in the proportion of fully extended chains with increasing macroscopic deformation gives rise to an overall non-affine deformation of the mean-square network-chain end-to-end distance and produces decreases in the shear modulus of the network at moderate macroscopic deformations, consistent with those observed experimentally. It may be noted that an increase in the proportion of fully extended chains can be viewed as an increase in the anisotropy of the (previously randomly oriented) array of network chains. This, coupled with the fact that the network model includes full molecular detail (bond lengths, valence angles, and bond-conformational energies), suggests that the segmental orientation and, thence, stress−optical properties of polymer networks can be investigated using this MC approach.

In the present paper, the stress−optical properties of cross-linked polyethylene (PE) networks are simulated. There is an abundance of experimental studies (see ref 2) of such networks, and also an established RIS model is available[21] to model the individual PE network chains. The detailed approach provides a deeper insight into the molecular origins of the observed stress−optical behavior, without the arbitrary assumptions of the Kuhn and Grün equivalent random-link model or the use of several parameters, as in the constrained-junction model.

Table 1. Calculated Dimensions of PE Chains, on with *n* Skeletal Bonds, at 403 K[a]

n	r_{max}/nm	$\langle r^2\rangle$/nm^2	m	n/m	l'/nm
40	5.07	5.79	4.45	9.00	1.14
60	7.61	9.14	6.34	9.47	1.20
80	10.15	12.49	8.24	9.71	1.23
100	12.68	15.84	10.16	9.85	1.25
140	17.76	22.55	13.99	10.01	1.27
180	22.83	29.24	17.83	10.10	1.28
220	27.91	35.94	21.66	10.16	1.29

[a] r_{max} is the fully extended end-to-end distance in the all planar-trans conformation; $\langle r^2\rangle$ is the mean-square end-to-end distance; m and l' are the numbers and lengths of equivalent freely jointed links, respectively.

Analysis of the Conformational and Orientation Behavior of *Individual* PE Chains

(i) MC Scheme. The MC algorithm described previously[20] was used to calculate the dimensions of individual PE chains of $n = 40$ to 220 skeletal bonds. The RIS parameters pertaining to the PE-chain structure were those of Abe, Jernigan and Flory.[21] MC sample sizes of 3×10^6 chain conformations were used, and the calculated values of the mean-square end-to-end distance, $\langle r^2\rangle$, differed from their *exact* RIS values, calculated using matrix algebra,[22,23] by less than 0.1%.

(ii) Dimensions of Equivalent Freely Jointed Chains. In order that the stress−optical properties of the PE networks calculated using the MC approach could be compared with the predictions of the Kuhn and Grün model used previously,[4] the parameters m and l' of the *equivalent* freely jointed chains for each of the "real" PE chains (n bonds of length l) were calculated. The method used was the conventional Kuhn treatment,[2] whereby the equivalent freely jointed chain is forced to adopt the same values of $\langle r^2\rangle$ and r_{max} as those of the real chain:

$$\langle r^2\rangle = ml'^2 \tag{1}$$

$$r_{max} = ml' \tag{2}$$

For a given PE chain, eqs 1 and 2 can be solved for m and l'. The method is limited to the analysis of chains with a single skeletal valence angle, such as PE, whose fully extended end-to-end distances, r_{max}, are calculable by simple geometry. The values of m, n/m, and l' for the series of PE chains investigated are listed in Table 1. It can be seen that the calculated values of n/m for the longer PE chains are in good agreement with the experimental value[24] of ca. 10. It may be noted that equivalent freely jointed chains can also be defined on the basis of higher-moment matching,[25,26] and this method generally yields much higher values of n/m (i.e. lower values of m for given values of n).

(iii) Distribution Functions of End-to-End Distance. Radial end-to-end distance distributions, $W(r)$, were formed as histograms, over the whole MC samples of chain conformations. The corresponding probability-density functions, $P(\boldsymbol{r})$, were calculated, using

$$P(\boldsymbol{r}) = \frac{W(r)}{4\pi r^2} \tag{3}$$

assuming random orientation of the end-to-end vectors, $\boldsymbol{r}$, for unperturbed chains. The elastic, Helmholtz free-energy of the chain[2] is $-kT \ln[P(\boldsymbol{r})]$. Plots of $\ln[P(\boldsymbol{r})]$ vs r/r_{max} for the series of PE chains are shown in Figure 1,

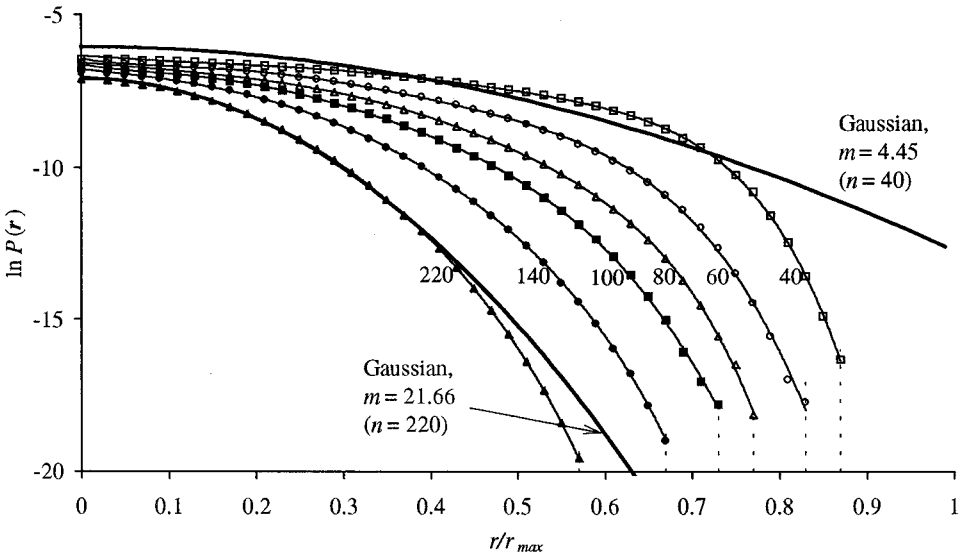

Figure 1. ln[$P(\boldsymbol{r})$] vs r/r_{max} for individual PE chains of $n = 40$ to $n = 220$ skeletal bonds, at 403 K. Plots for two Gaussian equivalent freely jointed chains of $m = 4.45$ ($n = 40$) and $m = 21.66$ ($n = 220$) links are also shown. --- indicates the values of r^*_{max} (see text).

where data-points are shown for each histogram interval of $r_{max}/50$. The MC data-points for the first histogram interval (centered at $r/r_{max} = 0.01$) are not shown, since, because $W(r) \rightarrow 0$ as $r \rightarrow 0$, the calculation of $P(\boldsymbol{r})$ according to eq 3 results in a degree of numerical uncertainty in ln[$P(\boldsymbol{r})$] as $r \rightarrow 0$. The intercepts of the MC curves with the Y axis in Figure 1 were therefore found by the extrapolation of plots of ln[$P(\boldsymbol{r})$] vs r^2, which are approximately linear in the region $r^2 \rightarrow 0$.

The Gaussian plots in Figure 1, for freely jointed chains with the same mean-square end-to-end distances, $\langle r^2 \rangle$, as the real PE chains, were calculated using the following equation:[2]

$$P(\boldsymbol{r}) = \left(\frac{3}{2\pi \langle r^2 \rangle}\right)^{3/2} \exp\left(\frac{-3r^2}{2\langle r^2 \rangle}\right) \qquad (4)$$

The use of ln[$P(\boldsymbol{r})$] as the ordinate emphasizes the differences between the simulated (MC) and Gaussian distributions, especially in the region of large chain extensions. The plot for $n = 40$ shows that the Gaussian values of $P(\boldsymbol{r})$ remain finite at chain extensions exceeding $r/r_{max} = 1$: a well-documented failing of the Gaussian model. As discussed previously,[20] the MC distributions show that conformations above a certain value of r (denoted r^*_{max}) occur with negligible probabilities (given that numbers are stored to six decimal places). Hence, in the MC samples of up to 3×10^6 chains, the values of $P(\boldsymbol{r})$ at $r = r^*_{max}$ are extremely small, on the order of 10^{-5} to 10^{-6} times the values at $r = 0$. For $r > r^*_{max}$, $W(r)$ is then effectively zero, and r^*_{max} is therefore the *effective conformationally* fully extended end-to-end distance of the real polymer chain. As the PE-chain length is increased from 40 to 220 skeletal bonds, the ratio r^*_{max}/r_{max} decreases.

Calculated Segmental-Orientation Functions

For each conformation sampled using the MC scheme, the orientations of individual $-CH_2-$ segment vectors, relative to the chain vector, were calculated. The segment vector, shown diagrammatically in Figure 2, is defined as the vector passing through the skeletal C atom in a direction parallel to the chain axis of an all-trans chain. More specifically, for the purposes of the current set of calculations, the vector for the ith segment lies in the plane of the ith and $(i-1)$th skeletal bonds, and at 34° to both bonds (since the C−C−C valence-angle supplement, $\theta = 68°$ for PE[21]). Therefore, a chain of $n + 1$ segments (n skeletal bonds) can be described in terms of $n - 1$ segment vectors ($i = 2$ to $i = n$). The orientation of each segment was defined by the angle ξ, between the ith segment and the end-to-end vector (see Figure 2).

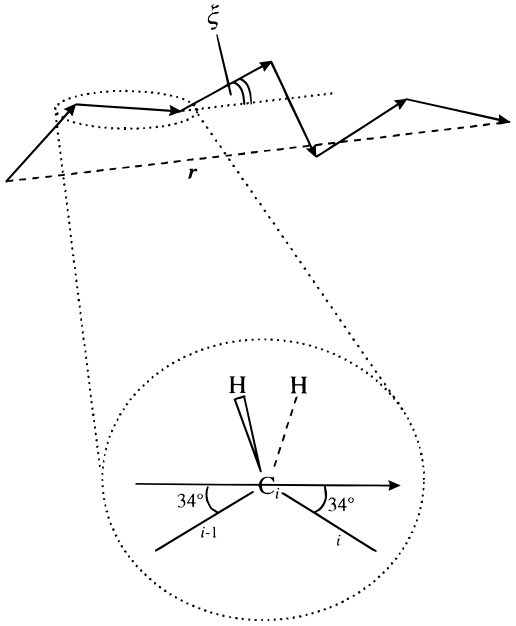

Figure 2. Illustration of the orientation angle ξ between a segment vector and the chain vector, $\boldsymbol{r}$.

Vector orientation is conventionally expressed in terms of the function (Legendre polynomial) $P_2(x)$, where[27]

$$P_2(x) = \frac{1}{2}(3\cos^2 x - 1) \qquad (5)$$

Alignment parallel with the reference direction occurs when $x = 0°$, $\cos^2 x = 1$, and $P_2(x) = 1$. Alignment

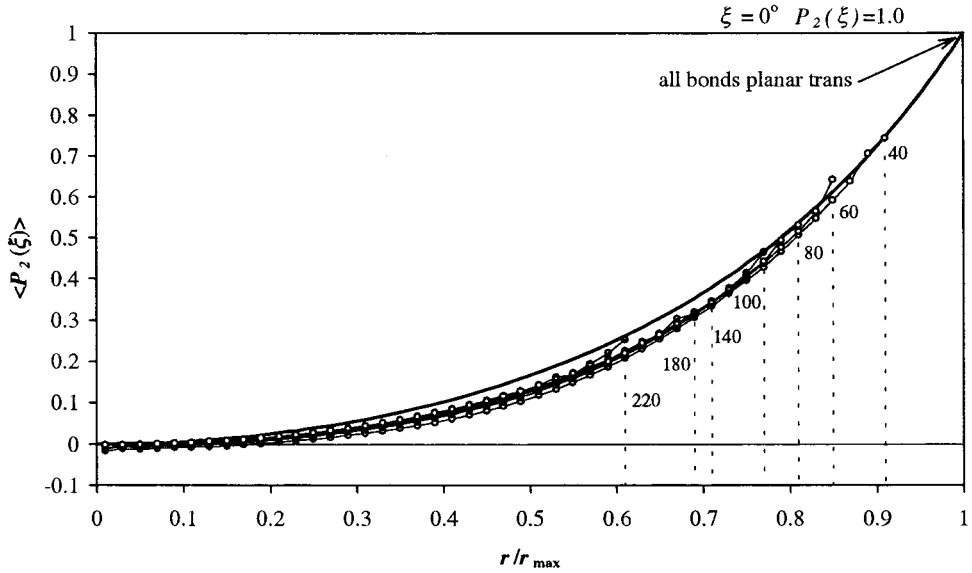

Figure 3. $\langle P_2(\xi)\rangle$ vs r/r_{max} for PE chains of 40−220 bonds, at 403 K. Dashed lines are drawn at r^*_{max}/r_{max} for each chain length, and the universal plot corresponding to the inverse Langevin approximation is shown as a solid curve.

perpendicular to the reference direction, i.e. $x = 90°$, occurs when $\cos^2 x = 0$, and $P_2(x) = -(1/2)$. A collection of vectors have random orientations when $\langle\cos^2 x\rangle = 1/3$, corresponding to $x = 54.73°$, and $P_2(x) = 0$.

For each chain conformation, the mean-square cosine, $\langle\cos^2 \xi\rangle$, averaged over all chain segments, was calculated, and $\langle\cos^2 \xi\rangle$ as a function of chain extension (r/r_{max}), was formed over the *total* MC sample of chain conformations. The variations of $\langle P_2(\xi)\rangle$ with r/r_{max} for PE chains of 40 to 220 skeletal bonds are shown in Figure 3. There is very little difference between the plots for different chain lengths, although they terminate at values of $r/r_{max} = r^*_{max}/r_{max}$ which decrease with increasing chain length (see dashed lines and Figure 1). It should be noted that *any* conformation, no matter how small its probability of occurrence, will contribute bonds to the calculation of $\langle P_2(\xi)\rangle$. As a result, the values of r^*_{max} recorded in this part of the calculation are slightly higher than those based on nonnegligible values of $W(r)$ and shown in Figure 1. The increased scatter in the orientation functions as $r \rightarrow r^*_{max}$ is due to the relatively small number of MC chain conformations sampled near r^*_{max}. As $r \rightarrow 0$, the chain becomes more highly coiled, any correlation between segment vectors and the chain end-to-end vector is reduced, and $\langle P_2(\xi)\rangle$ decreases. For the shorter PE chains ($n = 40$, 60, 80), $\langle P_2(\xi)\rangle$ becomes slightly *less than* zero as $r \rightarrow 0$. This is due to a finite chain-length effect in which $-CH_2-$ chain segments are not completely randomly oriented—there is a tendency toward the orientation of some segments *perpendicular* to the chain vector to facilitate the small chain end-to-end distances in this region of the distribution.

The solid curve in Figure 3 was calculated *analytically* for a freely jointed chain using the "inverse-Langevin" treatment.[2,23] Treloar[28] gives an expression for $\langle P_2(\xi)\rangle$, which is accurate to within ±1% over the entire range of r/r_{max} (=0 → 1):

$$\langle P_2(\xi)\rangle = \frac{1}{5}\left\{3\left(\frac{r}{r_{max}}\right)^2 + \left(\frac{r}{r_{max}}\right)^4 + \left(\frac{r}{r_{max}}\right)^6\right\} \qquad (6)$$

The inverse Langevin plot in Figure 3 is therefore universal, independent of the number of freely jointed links. The curves for the real PE chains lie just below the inverse Langevin curve, indicating, at a given chain extension, slightly less segmental orientation than for the freely jointed chain. However, it is clear that, as the PE-chain extension increases, the plots in Figure 3, as they should, tend to $\langle P_2(\xi)\rangle = 1$ at $r/r_{max} = 1$, which corresponds to $\xi = 0°$ for the fully extended, planar-trans conformation.

In Figure 4a, the average orientations for each segment are shown for unperturbed PE chains of 40 to 220 bonds, over all of the MC conformations generated (i.e. averaged over the whole, unperturbed end-to-end distance distribution). (For a chain of n skeletal bonds, the segment index, j, takes all integer values from 2 to n.) In the limit of infinite PE-chain length, the plot would lie along the abscissa ($\langle P_2(\xi_j)\rangle = 0$ for all j), corresponding to totally random segment orientation. However, for finite chain lengths, it is clear that, on average, segment orientations are partially correlated with the direction of the chain vector. Because of the fixed valence angles and preferred dihedral angles, there are also considerable "end effects", in which the directions of terminal segments are the least correlated with that of the end-to-end vector and segments toward the center of the chain become more aligned. This effect becomes more pronounced as the chain length is decreased. For each chain length, the average $\langle P_2(\xi)\rangle$ over the whole chain is shown by the horizontal dashed line.

The MC algorithm was modified to investigate the conformational properties of freely jointed chains of m links, using the same chain generation technique. Since only integer numbers of freely jointed links are suitable for the numerical analysis, the noninteger values of m in Table 1 were rounded up or down (as listed in Table 2), and the resulting set of freely jointed chains were investigated. In Figure 4b, the calculated $\langle P_2(\xi_j)\rangle$ values are plotted, showing the average orientation of links 1 to j. Due to the absence of valence-angle and dihedral-angle restrictions, end effects are not apparent in the freely jointed chains. However, like the PE chains, $\langle P_2(\xi_j)\rangle$ values are finite and only tend to zero in the limit $m \rightarrow \infty$. The scales of the ordinate axes in parts a and b of Figure 4 are identical, and it can be seen that the segmental orientation of a real (PE) chain is overesti-

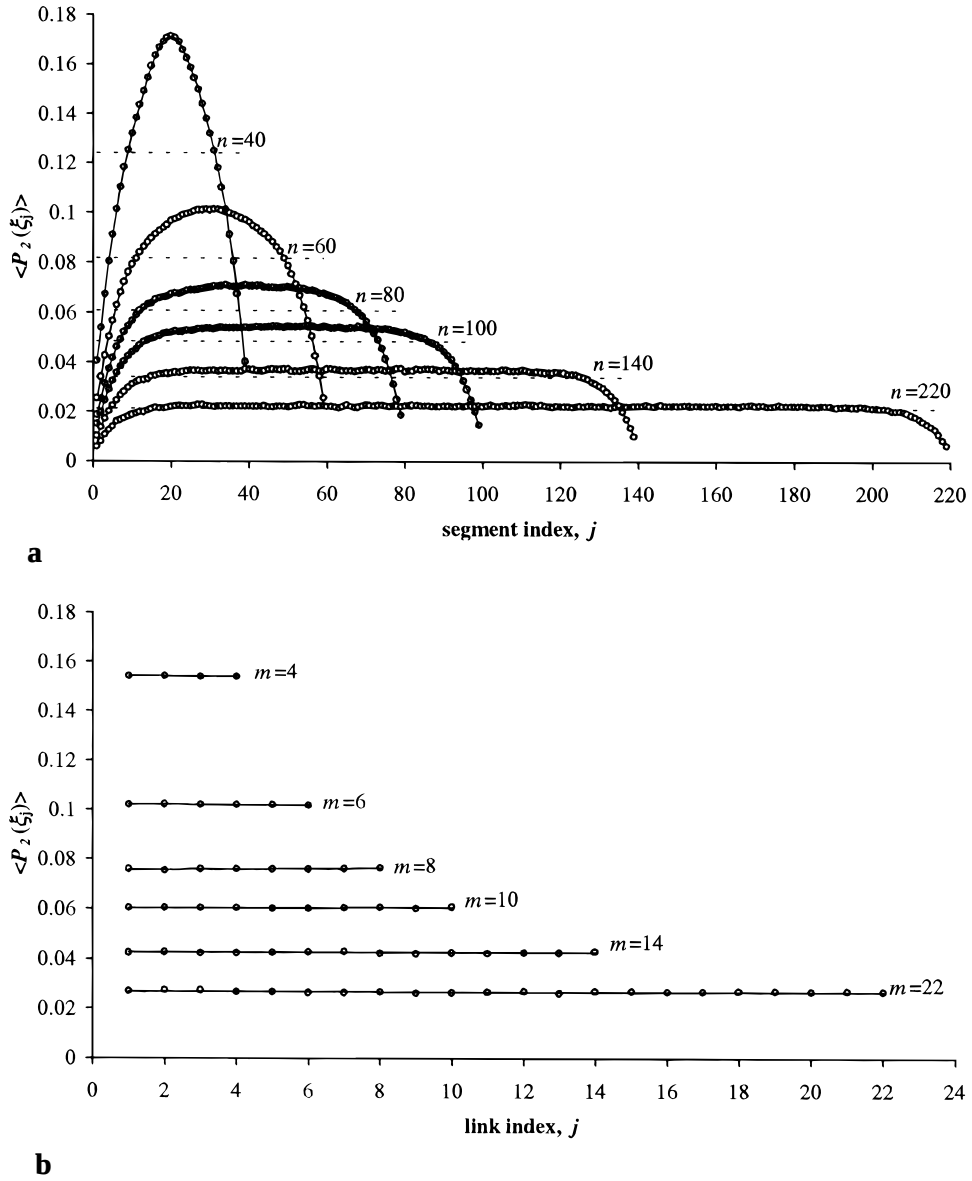

Figure 4. (a) $\langle P_2(\xi_j)\rangle$ for each segment, for PE chains of 40−220 skeletal bonds, at 403 K. The values of $\langle P_2(\xi_j)\rangle$ averaged over *all* segments are shown by the dotted lines. (b) $\langle P_2(\xi_j)\rangle$ for each link, for the set of approximately equivalent freely jointed chains of 4−22 links, for comparison with part a.

Table 2. Integer Numbers of Links, *m*, for the Set of Approximately Equivalent Freely Jointed Chains, Used for MC Analysis

n	*m*	*n*	*m*
40	4	140	14
60	6	180	18
80	8	220	22
100	10		

mated by considering its equivalent freely jointed counterpart, although the absolute differences decrease with increasing chain length.

Simulation of the Uniaxial Deformation of Networks of PE Chains

As described previously,[19,20] a model network consists of a random array of PE chains in three dimensions, with the conformational behavior of any individual network chain indistinguishable from that of an identical "free" chain. Upon the application of a macroscopic strain, each chain deforms affinely only up to $r = r^*_{max}$. Using an MC scheme, the elastic force is calculated from the total free-energy change resulting from the deformation of the end-to-end vectors of the collection of *individual* network chains, rather than from the uniform deformation of an "average" chain.[2,8,9]

The original network-deformation algorithm[20] was enhanced such that, for a given value of λ, concurrently with each chain-deformation, the orientation of the ith chain vector with respect to the applied strain, denoted $P_2(\psi_i)$, is calculated. Next, the value of $\langle P_2(\xi)\rangle_i$, for the average segment orientation with respect to the direction of the ith chain vector, is taken as equal to the value of $\langle P_2(\xi)\rangle$ at the calculated value of r/r_{max} for the given λ. In the event of a chain vector being extended beyond r^*_{max}, the magnitude of the deformed vector is set equal to r^*_{max}, thus defining the maximum value of $\langle P_2(\xi)\rangle_i$. However, the direction of the chain vector is allowed to rotate from the direction defined by (x_0, y_0, z_0) to that which would be defined by the affinely deformed chain, irrespective of the magnitude of r. The latter behavior is similar to the pseudoaffine deformation scheme described by Nobbs and Bower.[5]

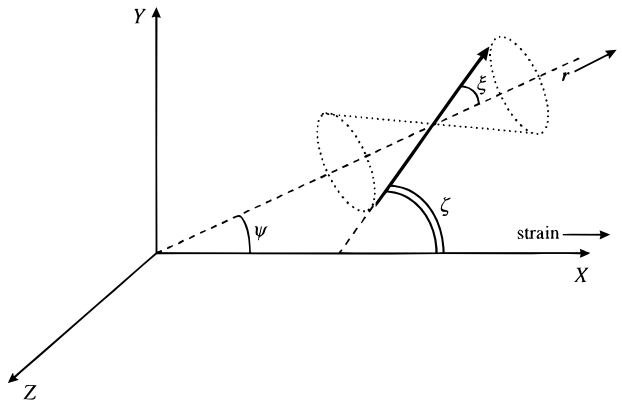

Figure 5. Illustration of orientation angles: ξ, between a segment vector and chain vector, $\boldsymbol{r}$; ψ, between $\boldsymbol{r}$ and the uniaxial strain direction; ζ, the effective angle between a segment vector and the strain direction. The segment is assumed to randomly occupy all positions on the cone defined by ξ, so that the calculated value of $P_2(\zeta)$ is an average, sampled over all cone positions of ξ.

For the MC sample of $N = 5 \times 10^6$ chains, the average chain-vector orientation, $\langle P_2(\psi_i)\rangle$, and average segment orientation, $\langle P_2(\xi)\rangle_i\rangle$, are formed, as a function of λ, using

$$\langle P_2(\psi_i)\rangle = \frac{1}{N}\sum_{i=1}^{N} P_2(\psi_i) \tag{7}$$

$$\langle\langle P_2(\xi)\rangle_i\rangle = \frac{1}{N}\sum_{i=1}^{N} \langle P_2(\xi)\rangle_i$$

Finally, using the Legendre addition theorem,[27] the average segmental orientation with respect to the direction of the applied uniaxial macroscopic strain, $\langle P_2(\zeta)\rangle$, was calculated from the convolution of the functions $\langle\langle P_2(\xi)\rangle_i\rangle$ and $\langle P_2(\psi_i)\rangle$ (see Figure 5), using the approximation

$$\langle P_2(\zeta)\rangle = \langle\langle P_2(\xi)\rangle_i\rangle \langle P_2(\psi_i)\rangle \tag{8}$$

Simulated Network Stress−Strain Behavior (Analysis of MC Results)

The normalized Helmholtz energy change for the array of ν chains, calculated as described previously,[19,20] can be expressed in terms of the density, ρ, and the volume, V, of the (unswollen) network using

$$\frac{\Delta A}{\nu kT} = \frac{\Delta A}{RT\rho}\frac{M_c}{V} = s\left(\lambda^2 + \frac{2}{\lambda} - 3\right) \tag{9}$$

where R is the universal gas constant, and M_c is the network-chain molar-mass. In general, s is a function of λ, although, for Gaussian network chains, $s = {}^1/_2$. Differentiation of eq 9 with respect to sample length, l, eventually yields[19,20] the normalized, true stress, $t/RT\rho$

$$\frac{t}{RT\rho} = \frac{1}{nM_0}\left\{2s\left(\lambda^2 - \frac{1}{\lambda}\right) + (\lambda^3 - 3\lambda + 2)\frac{\mathrm{d}s}{\mathrm{d}\lambda}\right\} \tag{10}$$

M_0 is the average molar mass per skeletal bond, such that $M_c = nM_0$. The simulated network stress, $t/RT\rho$, is plotted as a function of $\lambda^2 - \lambda^{-1}$, for networks of 40-bond to 220-bond PE chains in Figure 6. The linear plots for the Gaussian networks with the same values of M_c as the 40-bond and 220-bond PE network chains were calculated using eq 10, with $s = {}^1/_2$ and $\mathrm{d}s/\mathrm{d}\lambda = 0$. The initial slope (or shear modulus) for the simulated network of short (40-bond) PE chains is higher than that of the corresponding Gaussian plot, due to the markedly non-Gaussian character of the short PE chains (i.e. a finite chain-length effect, since n/m has not attained its limiting value). However, as PE-chain length increases, the stress−strain behavior tends toward that of the corresponding network of equivalent Gaussian chains. The *initial* modulus approaches that of the Gaussian network model. However, at higher extensions, the increasing proportion of conformationally fully extended PE chains causes a decrease in network modulus due to an exhaustion of the capacity for conformational-energy change.[19,20]

Network-Chain Orientation and Birefringence

The stress−optical coefficient, C, is defined as the ratio of the birefringence, $\Delta\tilde{n}$, and the true stress, t, as the deformation ratio, λ, tends to 1:

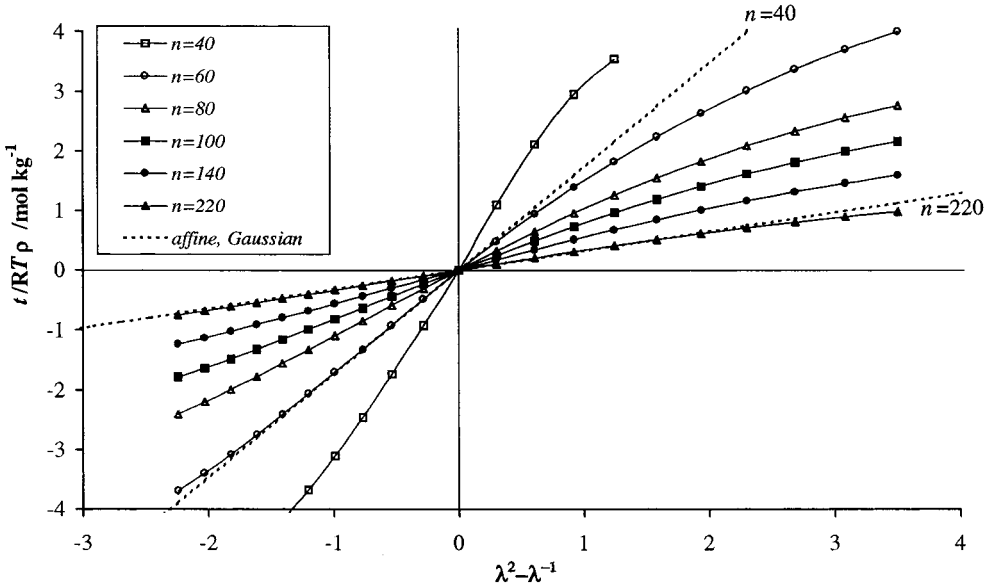

Figure 6. Normalized, true stress, $t/RT\rho$, vs $\lambda^2 - \lambda^{-1}$, for networks of 40-bond to 220-bond PE chains. For comparison, the plots for two networks of Gaussian chains, with the same network-chain molar masses (M_c) as the 40-bond and 220-bond PE chains, are also shown.

$$C = \left[\frac{\Delta\tilde{n}}{t}\right]_{\lambda\to 1} \tag{11}$$

Birefringence or double refraction refers to the difference in the refractive indices measured along mutually perpendicular sample axes and is given by

$$\Delta\tilde{n} = \tilde{n}_{\parallel} - \tilde{n}_{\perp} \tag{12}$$

where $\tilde{n}_{\parallel}$ and $\tilde{n}_{\perp}$ are refractive indices measured parallel and perpendicular to the direction of the applied strain, respectively. The values of $\tilde{n}_{\parallel}$ and $\tilde{n}_{\perp}$ are related directly to the orientations of polarizable units within a material (e.g., chemical bonds, polymer-chain segments) with respect to the direction of the applied strain. For uniaxial deformation, this orientation can be described by the angle ζ, defined previously, and $\Delta\tilde{n}$ is proportional to $\langle\cos^2\zeta\rangle$, averaged over the assembly of polarizable units. If p_1 and p_2 are the principal polarizabilities of each of the N polarizable units per unit volume, then the difference in *mean* polarizabilities per unit volume, parallel to and perpendicular to the deformation axis, is given by[29]

$$\langle p_{\parallel}\rangle - \langle p_{\perp}\rangle = N(p_1 - p_2)\langle P_2(\zeta)\rangle \tag{13}$$

where $\langle P_2(\zeta)\rangle = {}^1/_2(3\langle\cos^2\zeta\rangle - 1)$, as defined in eq 5. Using the mean polarizabilities and the Lorentz−Lorenz equation, the principal polarizabilities may be related to the birefringence as follows:[29]

$$\Delta\tilde{n} = \tilde{n}_{\parallel} - \tilde{n}_{\perp} = \frac{2\pi}{9}\frac{(\tilde{n}^2+2)^2}{\tilde{n}}N(p_1 - p_2)\langle P_2(\zeta)\rangle \tag{14}$$

$\tilde{n}$ is the refractive index averaged over all directions, and is equal to $(\tilde{n}_{\parallel} + 2\tilde{n}_{\perp})/3$. If all of the units were aligned parallel to the deformation axis, $\langle\cos^2\zeta\rangle = 1$ and the maximum possible birefringence, $\Delta\tilde{n}_{max}$, would be observed:

$$\Delta\tilde{n}_{max} = \frac{2\pi}{9}\frac{(\tilde{n}^2+2)^2}{\tilde{n}}N(p_1 - p_2) \tag{15}$$

By combination of eqs 14 and 15, $\langle P_2(\zeta)\rangle$ can be expressed in terms of the ratio of $\Delta\tilde{n}$ and $\Delta\tilde{n}_{max}$:

$$\langle P_2(\zeta)\rangle = \frac{\Delta\tilde{n}}{\Delta\tilde{n}_{max}} \tag{16}$$

In previous theoretical approaches,[1,2] the model was developed further to describe stress−optical behavior by making assumptions concerning the polymer-network structure. Assuming that the stress−strain behavior of the network is Gaussian, the true stress, t, is given by[2]

$$t = \frac{\rho RT}{M_c}(\lambda^2 - \lambda^{-1}) = \frac{\rho RT}{nM_0}(\lambda^2 - \lambda^{-1}) \tag{17}$$

The assumption that the network chains of n bonds can be replaced by freely jointed (Gaussian) chains consisting of m links also means that $\langle\cos^2\zeta\rangle$ can be determined analytically as a function of deformation,[30] using an expression due to Roe and Krigbaum:

$$\langle\cos^2\zeta\rangle = \frac{1}{3} + \frac{2}{15m}(\lambda^2 - \lambda^{-1}) \tag{18}$$

It may be noted that the right-hand-side of eq 18 contains the zeroth- and first-order terms of an infinite series, in which the higher terms are negligible when m is large ($m > 6$). For small values of m, inclusion of the higher terms results in a slight increase in the calculated value of $\langle\cos^2\zeta\rangle$.

Substituting for $\langle\cos^2\zeta\rangle$ in the expression for $\langle P_2(\zeta)\rangle$ (eq 5) gives

$$\langle P_2(\zeta)\rangle = \frac{1}{5m}(\lambda^2 - \lambda^{-1}) \tag{19}$$

In general, one may write

$$\langle P_2(\zeta)\rangle = Z_{\lambda}(\lambda^2 - \lambda^{-1}) \tag{20}$$

where Z_{λ} is the *deformation-orientation coefficient*, dependent upon the detailed network-chain structure and the density of the network. It is identical to the reduced orientation function, $[S]$, described by Besbes et al.[12] Thus, for a Gaussian network, Z_{λ} is equal to $1/5m$. However, it is important to note that the calculation of $\langle\cos^2\zeta\rangle$ according to eq 18 involves an evaluation of $\langle\cos^2\xi\rangle$ using individual chains, existing over the whole range of chain extensions, $r = 0$ to $r = r_{max}$ (see Figure 3), with segmental orientations described through the inverse-Langevin approach. The analysis of Roe and Krigbaum therefore predicts a *greater* average orientation than the numerical averaging performed in the MC analysis of "realistic" chains, whose maximum extension is restricted to r^*_{max} ($<r_{max}$) and, hence, results in lower values of $\langle P_2(\xi)\rangle$ and $\langle P_2(\zeta)\rangle$.

In Figure 7, the values of $\langle P_2(\zeta)\rangle$ evaluated from eq 8 for 40- to 220-bond PE networks, are shown as functions of $\lambda^2 - \lambda^{-1}$. The plots for the Gaussian networks were calculated via eq 19, using the values of m corresponding to the 40-bond and 220-bond PE chains given in Table 1. It is clear that the replacement of the real network chains by their equivalent Gaussian counterparts, as in the Kuhn and Grün scheme, and averaging segment orientations analytically over three dimensions[30] results in an overestimation of the segmental orientation in the deforming network, as expected. Even for the longest PE chain ($n = 220$), the simulated values of $\langle P_2(\zeta)\rangle$ are much lower than the Gaussian values with $m = 21.66$. For the shorter equivalent chains ($m = 4$, 6), inclusion of the higher terms in the calculation of $\langle\cos^2\zeta\rangle$ (eq 18) would yield even higher values of $\langle P_2(\zeta)\rangle$ and result in curved plots in Figure 7, whose gradients would increase with increasing macroscopic deformation. It should also be noted values of m defined on the basis of moment-matching[25] would be *lower* than those listed in Table 1, and would therefore result in even *greater* discrepancies between the MC and Gaussian plots.

The failings of the Gaussian network treatment are highlighted in Figure 8, where the initial slopes of the MC plots in Figure 7 (equal to Z_{λ}) are plotted as functions of $1/n$. The data points for the Gaussian network chains of m links are plotted at values of $1/n$ corresponding to their PE-chain equivalents. Thus, when account is taken of the finite extensibilities of network chains, as in the MC approach, Z_{λ}, the calculated deformation-orientation coefficient is markedly reduced relative to its value in the Gaussian-network approximation.

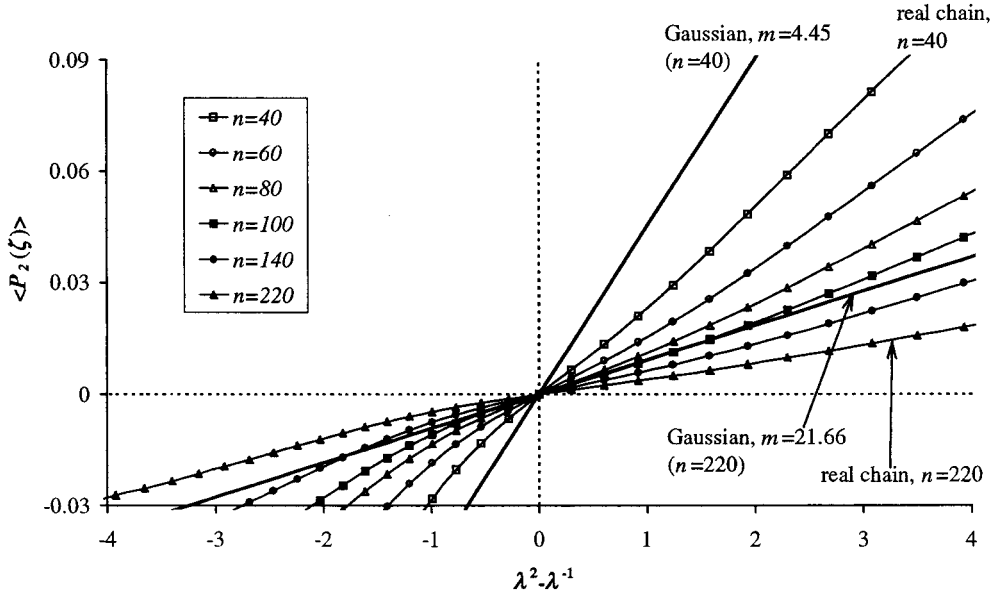

Figure 7. $\langle P_2(\zeta)\rangle$ vs $\lambda^2 - \lambda^{-1}$, for networks of 40-bond to 220-bond PE networks at 403K, and for Gaussian networks of freely jointed chains with $m = 4.45$ (equivalent to $n = 40$) and $m = 21.66$ (equivalent to $n = 220$).

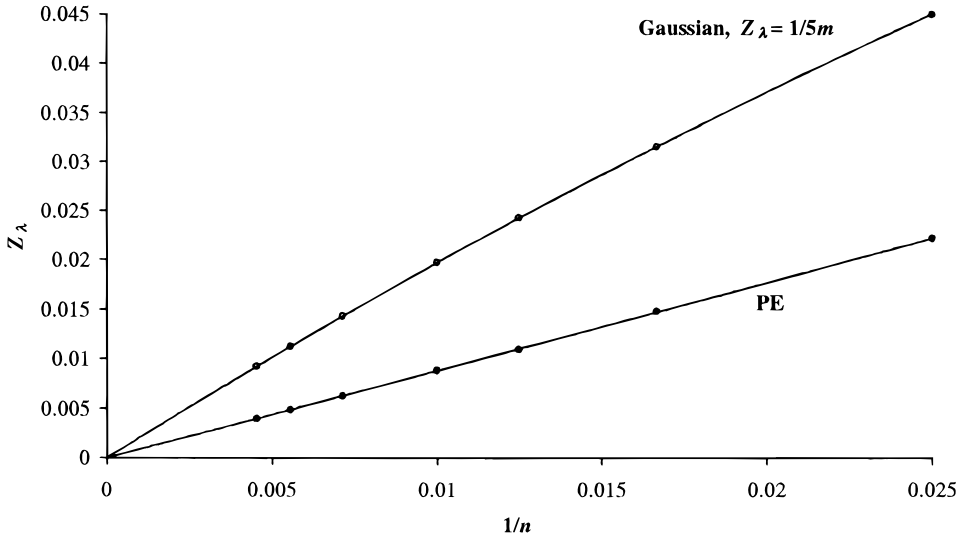

Figure 8. Deformation-orientation coefficients, Z_λ, as a function of $1/n$ for networks of PE chains of $n = 40$ to $n = 220$ bonds. The corresponding plot for the Gaussian networks of equivalent freely jointed chains (ranging from $m = 4.45$ to $m = 21.66$ links) is also shown.

The roles of segmental orientation and chain-vector orientation in determining the stress−orientation behavior of a network are illustrated in Figure 9. For a network of 100-bond PE chains, the values of $\langle P_2(\zeta)\rangle$ (calculated using eq 8) are shown as a function of λ. In addition, the *contributions* from segmental orientations with respect to the chain vector, $\langle P_2(\xi)\rangle$, and those from chain-vector orientation with respect to the strain axis, $\langle P_2(\psi)\rangle$, are shown. (*n.b.* the subscripts *i*, and the second set of brackets $\langle\ \rangle$, used in eq 8, have been dropped, to simplify the notation.) The chain-vector contribution ($\langle P_2(\psi)\rangle$) tends to 1 at high extensions, as expected, as all of the chain vectors become aligned parallel to the direction of the macroscopic strain. At high compressions, $\langle P_2(\psi)\rangle$ tends toward −0.5 as chain vectors become aligned *perpendicular* to the strain axis. $\langle P_2(\xi)\rangle$ will attain limiting values of unity in both extension *and* compression, but the magnitudes of the values of $\langle P_2(\xi)\rangle$ are much smaller than those of $\langle P_2(\psi)\rangle$ in the range of deformations studied. Accordingly, $\langle P_2(\zeta)\rangle$ is relatively small. The limiting, maximum value of $\langle P_2(\zeta)\rangle$ is equal to 1 in extension (corresponding to $\zeta = 0°$), and the limiting, minimum value is −0.5 in compression (corresponding to $\zeta = 90°$).

Stress−Orientation Behavior

Having dealt separately with the stress−strain properties and orientation−strain properties of the model PE networks, the combined stress−orientation behavior is now discussed. For PE network-chain lengths of 40−220 bonds, the normalized, true stress, $t/RT\rho$ (over the range $0.627 \le \lambda \le 1.5$), is plotted in Figure 10 against the corresponding value of $\langle P_2(\zeta)\rangle$. The plots are approximately linear at small strains, and the slopes increase with increasing network-chain length. In contrast, the Gaussian plots (calculated using eqs 17 and 19) for $m = 4.45$ and $m = 21.66$ are relatively insensitive to network-chain length. This behavior arises because the value of n/m only varies slowly with m. The failure

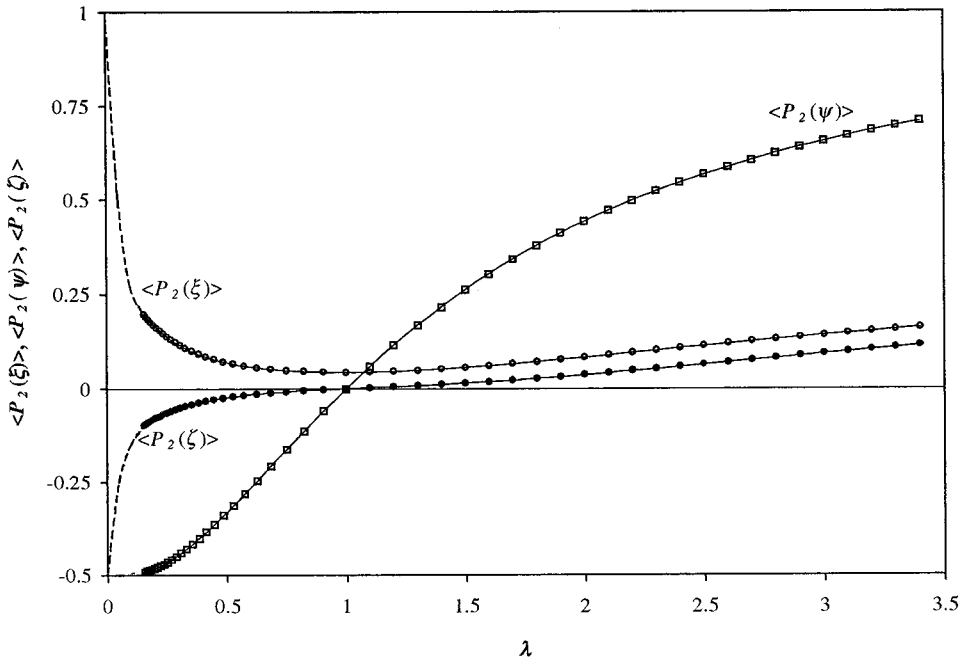

Figure 9. $\langle P_2(\zeta)\rangle$ vs λ for a network of 100-bond PE chains, showing the contributions from segment-to-chain-vector orientation, $\langle P_2(\xi)\rangle$, and from chain-vector orientation, $\langle P_2(\psi)\rangle$ are also shown.

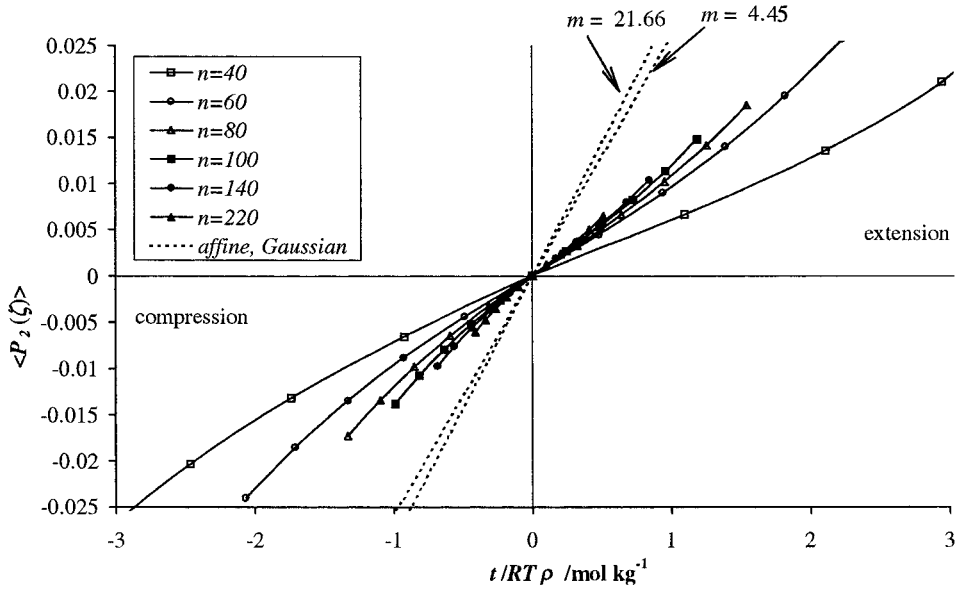

Figure 10. $\langle P_2(\zeta)\rangle$ vs $t/RT\rho$, for the networks of 40-bond to 220-bond PE chains at 403 K. Plots for networks of 21.66-link and 4.45-link Gaussian chains are shown for comparison.

of the Gaussian model is due to the fact that real network chains are replaced by freely jointed chains with no limit on chain extensibility. As expected, the slopes of the Gaussian plots are considerably larger than those of the MC plots, due to the overestimation of the segmental orientation, $\langle P_2(\zeta)\rangle$, when using the Gaussian model.

The initial slopes of the curves plotted in Figure 10 define a stress−orientation coefficient, Z_t, which can be related to the experimentally observed stress−optical coefficient:

$$Z_t = \left[\frac{\langle P_2(\zeta)\rangle \rho RT}{t}\right]_{\lambda\to 1} \tag{21}$$

For a Gaussian network (using eqs 17 and 19)

$$Z_t = \frac{M_c}{5m} = \frac{M_0}{5}\frac{n}{m} \tag{22}$$

Values of Z_t are plotted as functions of reciprocal network-chain length, $1/n$, in Figure 11. Again, the data points for Gaussian network chains of m links are plotted at values of $1/n$ corresponding to their PE-chain equivalents. The linear behavior for the model networks is similar to that of the experimentally observed stress−optical coefficient, C, for PE chains, which is also found to be[2,31] inversely proportional to $1/n$. It is clear that the Gaussian model would require much *larger* values of m if it were to reproduce the values of Z_t calculated using the MC method. The stress−orientation coefficients attain limiting values at infinite network-chain length of Z_t(PE) $\approx$ 0.013 kg mol^{-1}, and Z_t(Gaussian) $\approx$ 0.029 kg mol^{-1}.

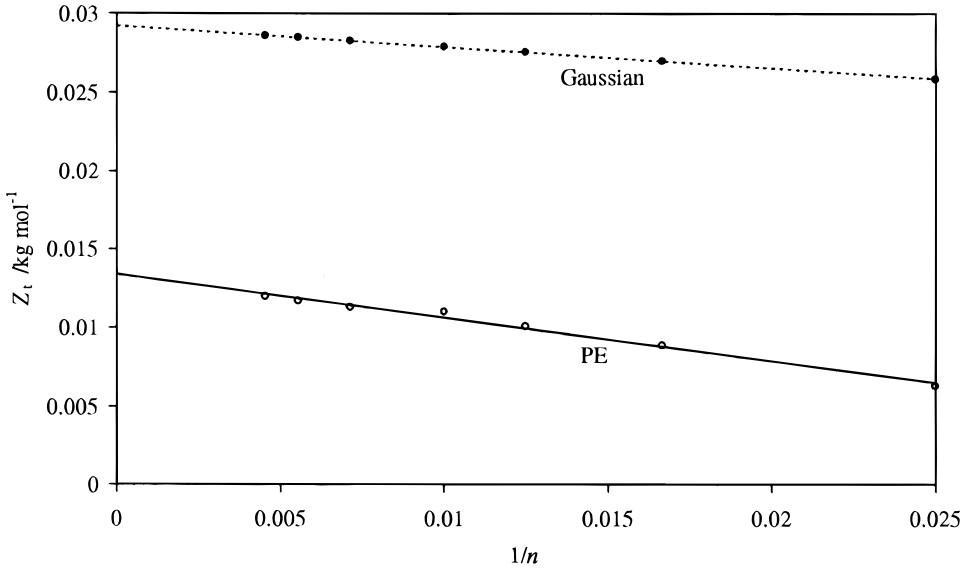

Figure 11. Plots of the stress−orientational coefficient, Z_t, vs 1/n, for networks of PE chains with $n = 40$ to $n = 220$, and the networks of equivalent Gaussian chains, all at 403K.

Table 3. Summary of the Experimental Stress−Optical Measurements of Saunders,[31] for Various PE Networks

primary molar mass/g mol^{-1}	radiation dose/ arbitrary units	M_c/g mol^{-1}	n	ρ/g cm^{-3}	C/cm^2 kg^{-1}
24000 (PE)	0.3	31830	2274	0.7924	2.00
24000 (PE)	0.6	12810	915	0.7937	1.93
24000 (PE)	2.0	3400	243	0.7987	1.59
24000 (PE)	4.0	1240	89	0.8061	1.10
32000 (PE)	0.3	16910	1208	0.7924	2.10
32000 (PE)	0.6	8070	576	0.7937	1.93
32000 (PE)	2.0	2960	211	0.7987	1.63
32000 (PE)	4.0	1200	86	0.8061	1.07
45000 (PE)	0.3	17700	1264	0.7924	2.20
45000 (PE)	0.6	8860	633	0.7937	2.09
45000 (PE)	2.0	3280	234	0.7987	1.66
45000 (PE)	4.0	1200	86	0.8061	1.14
PM	0	8930	638	0.7720	6.8
PM	0.06	3600	257	0.7720	6.7
PM	0.3	2920	209	0.7720	6.0
PM	1.0	1710	122	0.7720	5.1

Interpretation of the Experimentally Observed Stress−Optical Behavior of PE Networks

A seminal paper, describing the measurements of the photoelastic properties of a series of cross-linked PE networks was published by Saunders.[31] Three grades of PE with number-average molar masses of approximately 24 000, 32 000, and 45 000 g mol^{-1} and a sample of what is described as high molar-mass polymethylene (PM) were irradiated to various extents to yield cross-linked PE networks with different network-chain lengths (see Table 3). The experimental network-chain lengths, n, were estimated from the initial moduli, using the inverse-Langevin rubber elasticity theory (see Saunders[31] for description). The resulting values of n are also listed.

For each network sample, the true stress (t) and the birefringence ($\Delta\tilde{n}$) were measured as functions of λ, at temperatures of 403 K (for PE) and 453 K (for PM). In the range of deformations studied ($\lambda = 1$ to $\lambda \approx 2$), the plots of t vs $\Delta\tilde{n}$ were approximately linear, with gradients equal to the stress−optical coefficients, C. Saunders' results showed that C decreases markedly with increasing degree of cross-linking (i.e. decreasing network-chain length).

To compare the present calculated results for PE networks with the experimental data, it is necessary to define the relationship between the calculated stress−orientation coefficient (Z_t) and the experimentally measured stress−optical coefficient (C) or, in other words, the relationship between segmental orientation and birefringence. Equations 11, 16, and 21 show that

$$Z_t = \frac{C\rho RT}{\Delta\tilde{n}_{max}} \tag{23}$$

The experimental values of stress−optical coefficient C can thus be converted to the reduced stress−orientation coefficient, Z_t, using the experimental values of density, ρ, given in Table 3, T, and literature values for $\Delta\tilde{n}_{max}$. Two values of $\Delta\tilde{n}_{max}$ for the PE chain structure are often quoted. First, Denbigh[32] used measurements of the optical properties of gaseous CH_4 and C_2H_6 molecules to calculate bond polarizabilities for the $-CH_2-$ unit and hence $\Delta\tilde{n}_{max}$. A lower value of $\Delta\tilde{n}_{max}$ was later calculated by Bunn and Daubeny,[33] based on experimental measurements of the refractive indices of several paraffin crystals ($C_{32}H_{66}$, $C_{36}H_{74}$, $C_{38}H_{78}$). The difference between the values arising from the two sets of measurements has been discussed in detail elsewhere.[34] Using both sets of experimentally deduced bond polarizabilities, the present authors have recalculated $\Delta\tilde{n}_{max}$, based on a space-filling PE repeat-unit geometry,[35] to give $\Delta\tilde{n}_{max} = 0.223$ (Denbigh) and $\Delta\tilde{n}_{max} = 0.049$ (Bunn and Daubeny).

Using both $\Delta\tilde{n}_{max}$ values, the experimental values from Saunders for C were converted into values of Z_t using eq 23, and the results are plotted as functions of 1/n in Figure 12. It can be seen that the values of $\Delta\tilde{n}_{max}$ based on the bond polarizabilities of Bunn and Daubeny yield unrealistically high values of Z_t. On the other hand, the value of $\Delta\tilde{n}_{max}$ calculated using Denbigh's measurements yield experimental values of Z_t which are in closer agreement with the values from MC simulations. The experimentally observed decrease in Z_t with decreasing network-chain length is also approximately reproduced by the MC network model. Further, as shown in Figure 12, a value of $\Delta\tilde{n}_{max} \approx 0.375$ fits the experimental data almost exactly. Significantly, this value of $\Delta\tilde{n}_{max}$ is higher than that found by Denbigh.

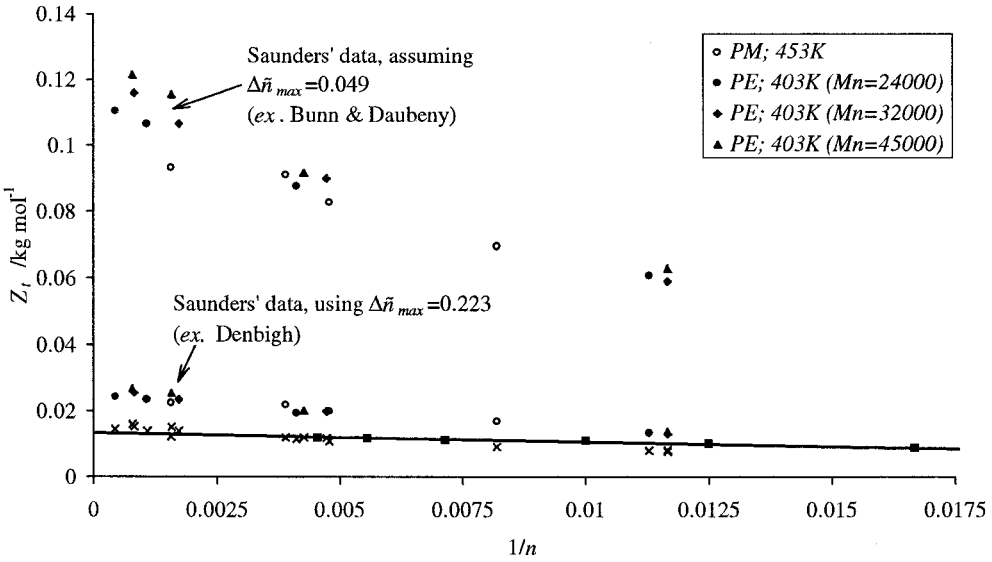

Figure 12. Z_t vs $1/n$ for model networks of 40-bond to 220-bond PE chains (−■−), compared with values derived[31] from Saunders' experimental values of C, calculated using $\Delta\tilde{n}_{max} = 0.049$ (Bunn, Daubeny), $\Delta\tilde{n}_{max} = 0.223$ (Denbigh), and $\Delta\tilde{n}_{max} = 0.375$ (×).

In the simulation studies, the calculated changes in network-chain segmental orientations are due wholly to the deformation of individual chain end-to-end vectors in the deforming network. Network-deformation experiments using NMR[13,15] and subsequent theoretical analyses[14−17] have shown that short-range, intermolecular orientational, or excluded-volume interactions can give rise to *additional* segmental orientation. As a result, the chains in a deforming network are likely to be locally more oriented than those of an individual-chain model. Importantly, the interacting-chain models developed by Sotta and Deloche[15,17] and by Brereton and Ries,[16] for example, yield increments to $\langle P_2(\zeta)\rangle$ that are linear in $\lambda^2 - \lambda^{-1}$ and inversely proportional to chain length. Such dependences are also true at small strains for the $\langle P_2(\zeta)\rangle$ values calculated using the individual-chain MC approach and for the Gaussian treatment. Thus, the fitting of MC and experimental data using the effective value $\Delta\tilde{n}_{max} = 0.375$ suggests that the fractional increase in $\langle P_2(\zeta)\rangle$, for network chains *in bulk*, is on the order of $0.375/0.223 \approx 1.7$, based on the value of $\Delta\tilde{n}_{max} = 0.223$ derived by Denbigh[32] from gas-phase birefringence data. This fractional increase in $\langle P_2(\zeta)\rangle$ is approximately of the order expected from theory.[36]

The Photoelastically Equivalent Freely Jointed Chain

The conformationally equivalent freely jointed chain, of m links, represents a real chain of n bonds and has the same values of $\langle r^2\rangle$ and r_{max}. The present work shows that the segmental orientation in a conformationally equivalent Gaussian chain is greater than that of the corresponding PE chain (see Figure 7). It is therefore useful to define an equivalent Gaussian chain of m^* random links. A network of such chains has the same stress−orientation properties as the real network.

Equating the expressions for Z_t for a real network (eq 21) and a Gaussian network (eq 22), and replacing m in eq 22 with m^*, yields

$$\frac{n}{m^*} = \frac{C\rho RT}{\Delta\tilde{n}_{max}}\frac{5}{M_0} = \frac{5Z_t}{M_0} \qquad (24)$$

It is clear that m^* evaluated through eq 24 is greater than m, since the segmental orientation in the Gaussian chains must be reduced in order to match Z_t calculated by the MC simulation of realistic PE chains. Since the real and conformationally equivalent freely jointed chains have identical values of $\langle r^2\rangle$ and r_{max}, the link length, l'^*, for the photoelastically equivalent freely jointed chain can be defined by matching *either* quantity (i.e. $\langle r^2\rangle = m^*(l'^*)^2$ or $r_{max} = m^* l'^*$). In both cases $l'^* < l'$.

The values for the numbers of real bonds per conformational and photoelastically equivalent random link, n/m and n/m^*, for equivalent chains defined on conformational and photoelastic bases, respectively, are plotted in Figure 13 as functions of $1/n$. The characteristics of the conformationally equivalent and photoelastically equivalent Gaussian chains obviously do not follow the same scaling with respect to n. The conformationally equivalent random link (l') is longer than the photoelastically equivalent random link (l'^*) defined on the basis of the Kuhn and Grün theory (i.e. $m < m^*$ for a given n). It is evident that the behavior of polymer networks cannot be described using a single equivalent freely jointed chain model to represent both their stress−strain *and* photoelastic properties. That is, more real skeletal bonds are needed for the vector directions of successive conformationally equivalent links to become uncorrelated than are needed for successive photoelastically equivalent links to become uncorrelated.

In all calculations carried out so far, the model networks have comprised monodisperse network chains. Current investigations are focusing on the effects of a *distribution* of network-chain lengths upon the calculated strain-orientation and stress−strain behaviors, and the results will be published in due course.

Concluding Comments

Computer simulation of the development of molecular orientation with extension ratio shows that the Kuhn and Grün model for the stress−optical behavior of a rubbery network is not realistic and is indeed very misleading in terms of physical understanding. Its deficiencies stem from the basic assumption that each molecular chain in a network can be replaced by an equivalent chain with a smaller number of freely jointed

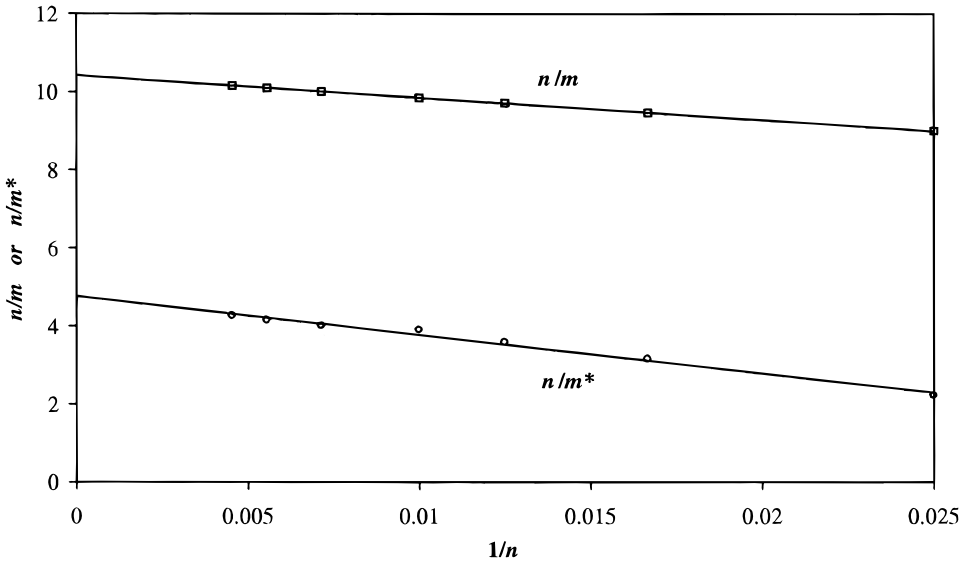

Figure 13. The number of real PE bonds, n, per equivalent freely jointed link, m, defined on the basis of Gaussian, conformationally equivalent chains, and m^*, defined on the basis of Gaussian, orientationally equivalent chains, plotted as functions of $1/n$.

links, with no limit on maximum chain extensibility. In the case of PE it has been shown that the Kuhn and Grün model grossly overestimates the molecular orientation. As a result, the apparent chain stiffness, expressed as n/m^*, is less than that expected from the chain-conformational statistics (n/m).

There are important technological implications arising from the realistic analysis presented in this paper. For example, the tensile-drawing behavior of a polymer, which is of vital importance to the production of fibers and films, has often been understood in terms of the stretching of the molecular network, whose junction points are formed by molecular entanglements. The maximum draw ratio achievable and, hence, the enhancement of physical properties such as modulus and strength relate to the limiting extensibility of this network. It is clear that because the Kuhn and Grün interpretation of stress−optical behavior yields an unrealistic number of equivalent freely jointed links per network chain, its use will provide an unreliable guide to the potential enhancement of properties which can be achieved by mechanical deformation. Awareness of this discrepancy has significant implications for polymer technology and polymer processing.

Acknowledgment. The authors wish to thank Dr. M. G. Brereton for useful discussions. The continuing support of the EPSRC (Grants GR/L 66649 and GR/L62306) is also gratefully acknowledged.

References and Notes

(1) Kuhn, W.; Grün, F. *Kolloid-Z.* **1942**, *101*, 248.
(2) Treloar, L. R. G. *The Physics of Rubber Elasticity*, 3rd ed.; Clarendon Press: Oxford, England, 1975.
(3) For example, see: Saunders: D. W. *Trans. Faraday Soc.* **1957**, *53*, 860.
(4) Nobbs, J. H.; Bower, D. I.; Ward, I. M. *J. Polym. Sci.: Polym. Phys. Ed.* **1979**, *17*, 259.
(5) Nobbs, J. H.; Bower, D. I. *Polymer* **1978**, *19*, 1100.
(6) Kratky, O. *Kolloid Z.* **1933**, *64*, 213.
(7) Flory, P. J., *J. Chem. Phys.* **1977**, *66*, 5720.
(8) Flory, P. J.; Erman, B. *Macromolecules* **1983**, *16*, 1601.
(9) Flory, P. J.; Erman, B. *Macromolecules* **1983**, *16*, 1607.
(10) For example, see: Erman, B.; Bahar, I.; Besbes, S.; Bokobza, L.; Monnerie, L. *Polymer* **1993**, *34*, 1858.
(11) For example, see: Buffeteau, T.; Desbat, B.; Besbes, S.; Nafati, M.; Bokobza, L. *Polymer* **1994**, *35*, 2538.
(12) Besbes, S.; Cermelli, I.; Bokobza, L.; Monnerie, L.; Bahar, I.; Erman, B.; Herz, J. *Macromolecules* **1992**, *25*, 1949.
(13) Sotta, P.; Deloche, B.; Herz, J. *Polymer* **1988**, *29*, 1171.
(14) Brereton, M. G. *Macromolecules* **1993**, *26*, 1152.
(15) Sotta, P.; Deloche, B. *Macromolecules* **1990**, *23*, 1999.
(16) Brereton, M. G., Ries, M. E., *Macromolecules*, **1996**, *29*, 2644.
(17) Sotta, P.; Depner, M.; Deloche, B. *Polym. Sci., Ser. A* **1996**, *38* (1), 71.
(18) See: Flory, P. J.; Chang, W. C. *Macromolecules* **1976**, *9*, 33.
(19) Stepto, R. F. T.; Taylor, D. J. R. *Macromol. Symp.* **1995**, *93*, 261.
(20) Stepto, R. F. T.; Taylor, D. J. R. *J. Chem. Soc., Faraday Trans.* **1995**, *91*, 2639.
(21) Abe, A.; Jernigan, R. L.; Flory, P. J. *J. Am. Chem. Soc.* **1966**, *88*, 631.
(22) Mattice, W. L.; Suter, U. W. *Conformational Theory of Large Molecules*, John Wiley & Sons Inc.: New York, 1994.
(23) Flory, P. J. *Statistical Mechanics of Chain Molecules*; Interscience: New York, 1969.
(24) Chiang, R. *J. Phys. Chem.* **1965**, *69*, 1645.
(25) Hill, J. L.; Stepto, R. F. T. *Trans. Faraday Soc.* **1971**, *67*, 3202.
(26) Yoon, D.; Flory, P. J. *J. Chem. Phys.* **1974**, *51I*, 5366.
(27) Ward, I. M. *Adv. Polym. Sci.* **1985**, *66*, 81.
(28) Treloar, L. R. G. *Trans. Faraday Soc.* **1954**, *50*, 881.
(29) Ward, I. M. *Br. J. Appl. Phys.* **1967**, *18*, 1165.
(30) Roe, R. J.; Krigbaum, W. R. *J. Appl. Phys.* **1964**, *35*, 2215.
(31) Saunders: D. W. *Trans. Faraday Soc.* **1956**, *52*, 1425.
(32) Denbigh, K. G. *Trans. Faraday Soc.* **1940**, *36*, 936.
(33) Bunn, C. W.; Daubeny, R. de P. *Trans. Faraday Soc.* **1954**, *50*, 1173.
(34) Volkenstein, M. V. *Configurational Statistics of Polymeric Chains*; English Translation; Timasheff, S. N., Timasheff, M. J., Eds.; Interscience: New York, 1963; Chapter 7.
(35) Appleyard, A.; Stepto, R. F. T. Unpublished data. Space-filling PE-chain geometry: ∠CCC = 112°, ∠CCH = 109.47° (tetrahedral), and ∠HCH = 106.82°.
(36) Private discussions with M. G. Brereton.

MA9805001